Heralds of a Future Eruption? Swarms of Microseismicity beneath the submarine Kolumbo Volcano indicate Opening of near-vertical Fractures exploited by ascending Melts

F. Schmid[1], G. Petersen[2], E. Hooft[3], M. Paulatto[4], K. Chrapkiewicz[4], M. Hensch[5], T. Dahm[2]

[1]GEOMAR Helmholtz-Centre for Ocean Research Kiel, Germany
[2]GFZ Helmholtz-Centre Potsdam, German Research Centre for Geosciences Potsdam, Germany
[3]University of Oregon, Eugene, USA
[4]Imperial College London, Department of Earth Science and Engineering, Prince Consort Road, UK
[5]Geological Survey of Baden-Württemberg, Freiburg, Germany
[6]National and Kapodistrian University of Athens, Department of Geology and Geoenvironment, Athens, Greece

Keywords: Aegean, Hellenic Volcanic Arc, Santorini, submarine volcanism, earthquake swarms

Key Points:

- Seismicity is densest in a cone-shaped volume of the crust beneath Kolumbo; the cone's tip coincides with a melt reservoir at 2-4 km depth
- Seismicity swarms occupy nearby, yet different portions of the crust
- Swarms likely triggered by combination of fluid pressure perturbations and redistribution of elastic stresses

Abstract

The Kolumbo submarine volcano in the southern Aegean (Greece) is associated with repeated seismic unrest since at least two decades and the causes of this unrest are still hardly understood. We present a ten-month long microseismicity dataset for the period 2006-2007. The majority of earthquakes clusters in a cone-shaped portion of the crust below Kolumbo. The tip of this cone coincides with a low Vp-anomaly at 2-4 km depth, that is interpreted as a crustal melt reservoir. Our dataset includes several earthquake swarms, of which we analyse the four strongest in detail. The swarms occupy near-vertical volumes of the crust and together they form a zone of fracturing elongated in SW-NE direction, parallel to major regional faults. All four swarms show a general upward migration of hypocentres and the cracking front propagates unusually fast, compared to swarms in other volcanic areas. We conclude that the swarm seismicity is most likely triggered by a combination of pore-pressure perturbations and the re-distribution of elastic stresses. Fluid pressure perturbations are induced either by obstructions in the melt conduits in a rheologically strong layer between 6-9 km depth or by dynamic triggering from purely tectonic earthquakes. We conclude that the zone of fractures below Kolumbo is exploited by melts ascending from the mantle and filling the crustal melt reservoir. Together with the recurring seismic unrest, our study suggests that a future eruption is feasible and monitoring of the Kolumbo volcanic system is highly advisable.

1 Introduction

Submarine volcanic eruptions in shallow waters often associate with violent phreatomagmatic explosions and have the potential to generate destructive tsunamis (e.g. Colgate and Sigurgeirsson, 1973; Moore, 2009; Starostin et al., 2005). Persistent volcanic unrest is a common precursor to volcanic eruptions (Phillipson et al., 2013). The edifice of the Kolumbo submarine volcano in the southern Aegean (Greece) lies only 50-500 meters below the sea surface (Fig. 1a). During the past two decades the crust below Kolumbo has been characterized by persistent seismic unrest (Fig. 2; Andinisari et al., 2021a; Bohnhoff et al., 2006; Dimitriadis et al., 2010; Dimitriadis et al., 2009). The causes of this seismic unrest are still poorly understood and there is an ongoing debate about the potential of future eruptions at Kolumbo. Geochemical data from hydrothermal fluids vented inside the Kolumbo crater indicate an elevated magmatic activity beneath Kolumbo, compared to the melt plumbing system below Santorini and other terrestrial volcanic systems (Rizzo et al., 2019). However, a conceptual model of the magma chamber below Kolumbo assumes a steady but slow replenishment with mantle melts and suggests an eruption in the near future is unlikely (Konstantinou, 2020).

We present the results of a ten-month long deployment of ocean bottom stations that recorded several thousand small earthquakes (Mw 0.0-3.7), including multiple earthquake swarms beneath Kolumbo. We located the earthquakes in a 3D velocity model and achieved hypocenter locations of high accuracies. The earthquake locations, together with moment tensor inversions and a recently acquired seismic image of a shallow melt reservoir below Kolumbo allow studying the magma plumbing system beneath Kolumbo in unprecedented detail. Our results are crucial to evaluate the state of the volcanic system and the potential volcanic hazards and highlight the need for continuous volcanic and seismologic monitoring.

Considering the dense population of the nearby Santorini Archipelago (~17.500 inhabitants) and the large number of tourists visiting this area (~2 million per year), a robust assessment of the volcanic hazards associated with Kolumbo is of societal and economic relevance.

Earthquake swarms in volcanic settings

Seismicity swarms are defined as sequences of earthquakes clustered in space and time that do not follow a simple Omori law (Shcherbakov et al., 2004) but contain multiple earthquakes of similar magnitude. Earthquake swarms do not scale with the total seismic moment released (Passarelli et al., 2018), suggesting that their evolution over time is modulated by transient processes, for example fluid migration, magmatic intrusions or aseismic slip acting in addition to long-term tectonic stresses (Passarelli et al., 2018; Vidale and Shearer, 2006). In volcanically and geothermally active regions earthquakes swarms are commonly observed and their study can be very beneficial to better understand the active processes in those systems (Hainzl, 2004; Shelly et al., 2013; Yukutake et al., 2011), motivating us to perform a detailed analysis of earthquake swarms recorded below Kolumbo.

2 Geological Setting of Kolumbo and Eruption History

The Christiana-Santorini-Kolumbo volcanic field represents the most active volcanic system in the eastern Mediterranean. It produced more than 100 explosive eruptions during the past 650 ka (Druitt et al., 2019; Kutterolf et al., 2021). The volcanic field includes the inactive Christiana volcanic edifice, the iconic Santorini Caldera and the submarine Kolumbo volcano (Fig. 1; Nomikou et al., 2019). All three volcanoes are aligned parallel to a SW-NE striking zone of extensional basins in the Hellenic Volcanic Arc that results from the subduction of the African Plate under the Aegean Microplate (Papanikolaou, 2013). The submerged Kolumbo volcano is located ~7 km to the northeast off the coast of Thera and represents the largest volcano in a chain of about 24 volcanic cones that follow the SW-NE trend of the trans-tensional Anhydros Basin (Fig. 1; Hooft et al., 2017; Nomikou et al., 2016; Nomikou et al., 2012).

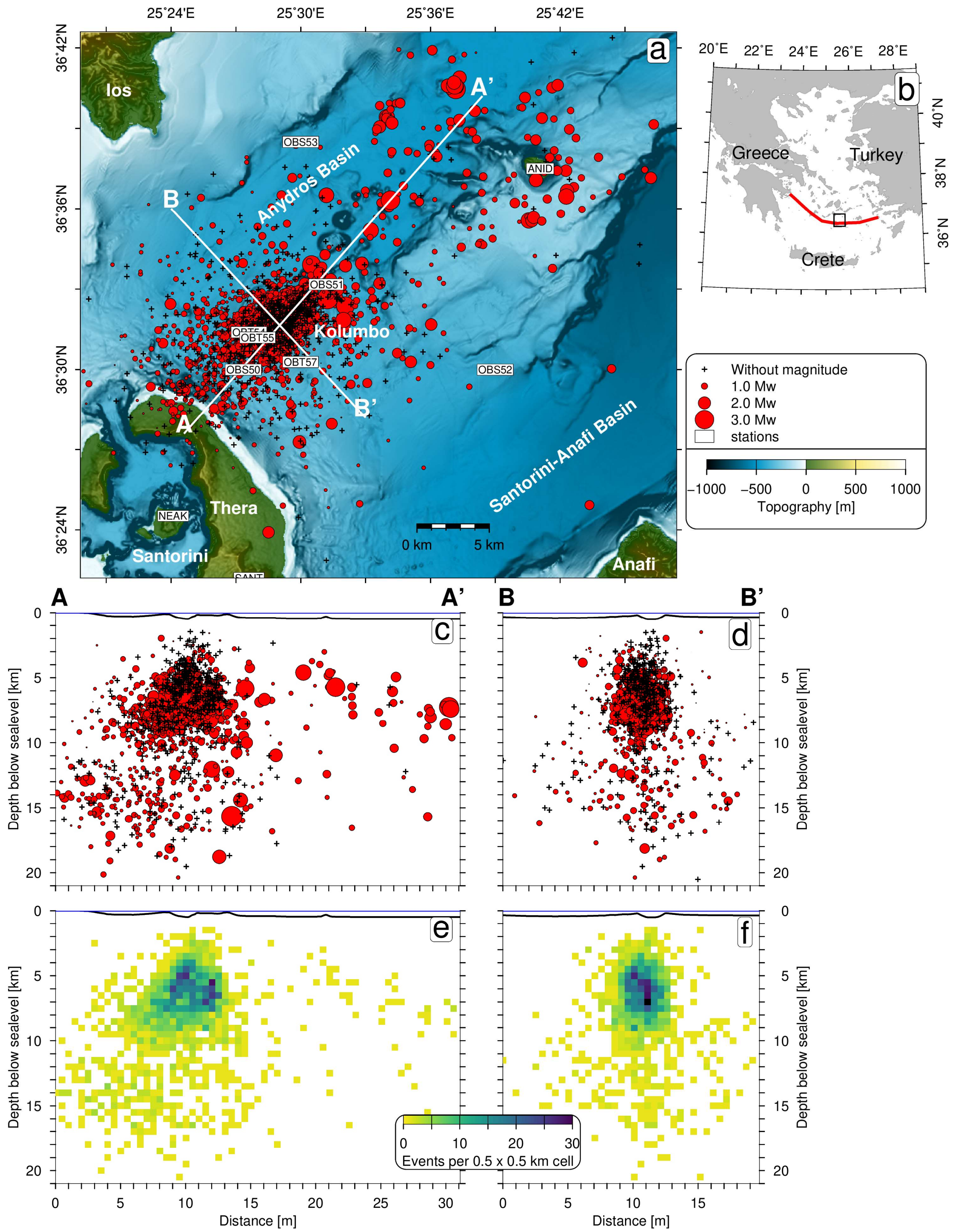

Figure 1. *a) Topography and bathymetry of the Santorini Kolumbo region with epicentres of seismicity in the period 2006/06-2007/03. Bathymetry data from Hooft et al. (2017). b) Overview of the Aegean Sea with the Hellenic Volcanic Arc indicated by heavy orange line and black square indicating perimeter of panel a. Panels c and d show cross-sections with projected hypocentres from earthquakes that are within 2 km of the profile (white lines in map a). Panels e and f show gridded event density for events plotted in panels c and d.*

The latest eruption of Kolumbo dates to the year 1650 AD and was documented by eyewitness (Cantner et al., 2014; Fouqué, 1879). This eruption of submarine and subaerial explosive activity lasted four months and resulted in ~70 fatalities on Santorini, caused mainly by volcanic gases released during the eruption (Cantner et al., 2014). The eruption peaked in phreatomagmatic explosions that caused a tsunami of regional impact and shaped the present day crater of ~2 km diameter and ~ 0.5 km depth (Cantner et al., 2014; C. Hübscher et al., 2015; Nomikou et al., 2014). Reflection seismic profiles crossing the Kolumbo edifice revealed five circular, stacked, cone-shaped, units, with the uppermost one deposited during the 1650 AD eruption (C. Hübscher et al., 2015; Preine et al., 2021). Precise dating is only available for the latest eruption of Kolumbo. However, a recently established regional stratigraphic framework of the entire CSKVF region estimates that the deposits of older eruptions have approximate ages of 0.35 Ma, 0.45 Ma, 0.9 Ma and older than 1.0 Ma (Preine et al., 2021).

Geochemical and mineralogical signatures of eruptive products of the 1650 AD eruption of Kolumbo suggest that the magma plumbing system of Kolumbo is independent from the magma plumbing system of Santorini (Francalanci et al., 2005; Klaver et al., 2016). Thermo-barometric analyses of fluid inclusions in erupted rocks from the 1650 AD eruption of Kolumbo indicate a pre-eruption storage at ~6 km depth assuming a H_2O saturated magma (Cantner et al., 2014).

A conceptual model of the Kolumbo magma plumbing system was developed by Konstantinou (2020) that infers a constant replenishment of the crustal magma chamber by melts ascending from the mantle. Andinisari et al. (2021a) and Konstantinou (2020) hypothesize that the clustered seismicity at 5-16 km depth beneath Kolumbo reflects this replenishment. All these findings underline that Kolumbo is still in a phase of volcanic activity. Passive seismological experiments using data from 2002-2005 found a low velocity anomaly at 5-7 km depth beneath Kolumbo that was interpreted as magma chamber (Dimitriadis et al., 2010). First arrival time tomography from a more recent active seismic experiment in 2015 found only slightly reduced velocities between 3 to 5 km depth beneath Kolumbo, consistent with little to no melt (0-1%) (McVey et al., 2019). However, full-waveform inversion of the same dataset identified a low Vp anomaly of limited spatial extent at 2.1-4.0 km depth below sealevel which is interpreted as volume of partial melts with melt fractions of 28-44% (Chrapkiewicz et al., in review).

Repeated clusters of local earthquakes underneath Kolumbo during the previous decades at depths of 5-20 km were interpreted as seismic unrest, related to the migration of magmatic fluids in and below the crustal magma chamber (Fig. 2; Andinisari et al., 2021a; Bohnhoff et al., 2006; Dimitriadis et al., 2009). The seismic unrest continues until today, and is recorded in the seismicity dataset of the National Observatory of Athens (https://bbnet.gein.noa.gr/HL/databases/database) from which we plot all events occurring in the Santorini-Kolumbo region during the recent two decades (Fig. 2).

Dives of remotely operated vehicles inside the Kolumbo crater discovered a field of active hydrothermal chimneys near the northern crater wall, vigorously venting fluids that are up to 220° C hot and consist of almost pure CO_2 (Carey et al., 2013; Kilias et al., 2013; Rizzo et al., 2016; Sigurdsson et al., 2006). Rizzo et al. (2019) presented detailed geochemical analyses of fluids vented by the hydrothermal chimneys inside Kolumbo. They identified unusual concentrations of Hg(0) that are strongly elevated compared to hydrothermal fluids sampled at Santorini or other terrestrial volcanoes and may be interpreted as further evidence – in addition to the persistent seismic unrest – for the high level of on-going magmatic activity below Kolumbo.

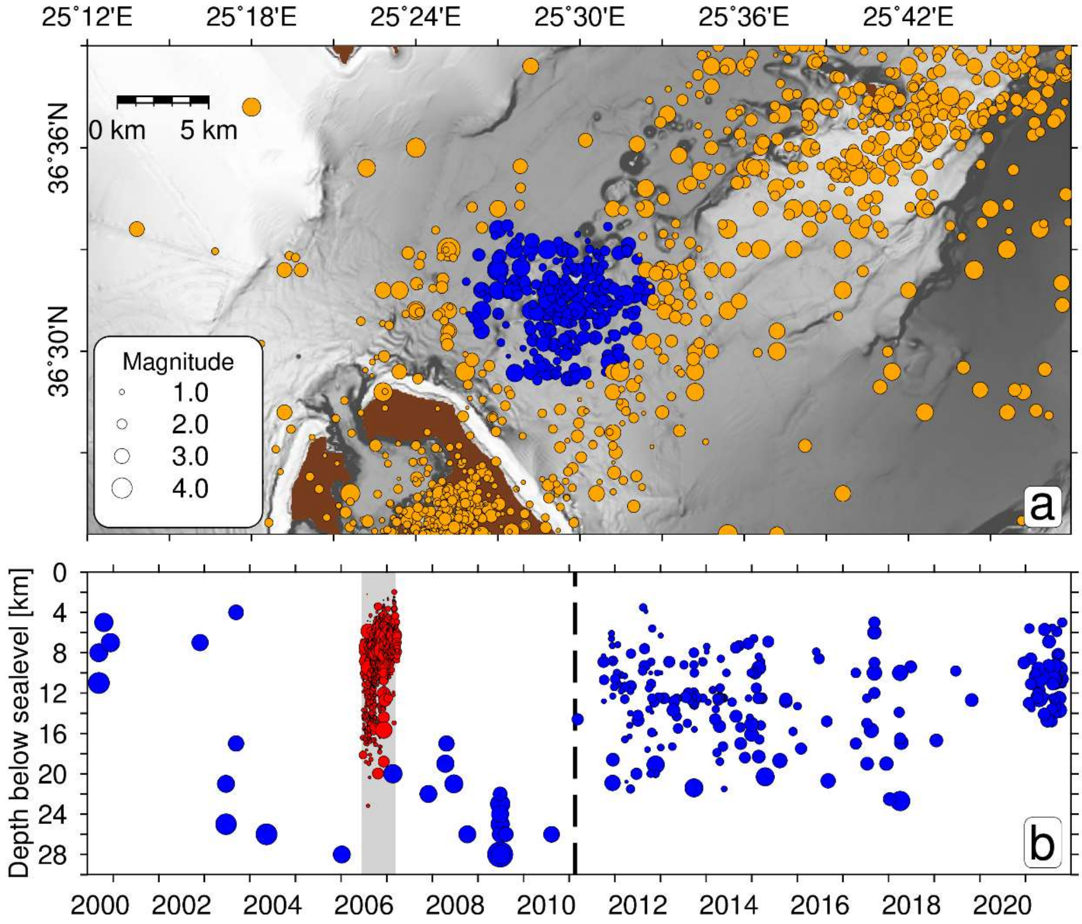

Figure 2. *a) Epicentres of earthquakes between 2000-2021 in the study area retrieved from the National Observatory of Athens (https://bbnet.gein.noa.gr/HL/databases/database; accessed 11/2021). Blue epicentres are within 5 km of Kolumbo and were included in panel b. b) Time versus depth distribution of seismicity near the Kolumbo. The grey area indicates the period considered in this study and red hypocentres represent all earthquakes in our dataset located closer than 5 km from Kolumbo (Fig. 1a). Note, the red hypocentres in panel b are not included in panel a, for clarity. In the dataset from the National Observatory of Athens the lower cut-off magnitude has shifted to smaller magnitudes over time. Before 2011 the dataset only included earthquakes of magnitude ≥ 3.0. From early 2011 onwards (indicated by the dashed vertical line) the seismicity dataset is complete for magnitude ≥ 2.0.*

3 Data and Methods

3.1 Seismic Networks, Data and Processing

Two synchronously operated temporal networks provided the seismic data presented in this study. The first one (project EGELADOS) consisted of 47 broadband land stations and seven short-period seismometers, operated from October 2005 to March 2007 (Friederich and Meier, 2008). A smaller network of eight ocean bottom instruments was deployed in the Anydros Basin by the University of Hamburg and operated from June 2006 to March 2007 (Hensch, 2009; C Hübscher et al., 2006). This network included four ocean bottom seismometers with hydrophones (OBS-H) and four ocean bottom tiltmeters with hydrophones (OBT-H). A map of all stations used in this study is included in the Supplements (Fig. S1).

3.2 Database handling and Phase Onset Picking

We used the hydrophone channels of the ocean bottom stations and a classical short-term-average versus long-term-average trigger for detecting seismic. This process resulted in approximately 5000 network detections. For each network trigger the waveforms of all stations (ocean bottom stations plus land stations) were extracted and registered in a database, managed through the Seisan software (Havskov and Ottemoeller, 1999). We picked the onsets of P and S phases manually. To determine the uncertainties associated with traveltime picking we picked each phase two times, at the first and last plausible onset time. The time difference then provided the picking uncertainty and the average of the two picks was used as input information for the hypocenter location. Average picking uncertainties were 0.05 s for P phases and 0.11 s for S phases.

3.3 Location of Hypocentres with NonLinLoc using a 3D velocity model

For the hypocentre location procedure we used the non-linear location software NonLinLoc (Lomax et al., 2000) which includes the highly efficient Oct-Tree grid-search algorithm (Lomax and Curtis, 2001). In the location procedure we only included events that have phase onset picks from at least five stations and include at least two S phase arrivals. As NonLinLoc allows the utilization of 3D velocity models we included the regional 3D Vp model of Heath et al. (2019) and McVey et al. (2019) that was generated by travel time tomography from active source data of the PROTEUS experiment (2015) and covers a large part of the Santorini-Amorgos region. Since some stations were outside the 3D Vp model of Heath et al. (2019) we extrapolated the model to cover the entire network used in this study, see Supplements Figure S1. For Vs velocities we created a 3D grid of identical dimensions as the 3D Vp grid and derived Vs velocities through a fixed Vp/Vs ratio of 1.77, which was estimated from a Wadati-diagram, included in Hensch (2009). This value is in agreement with the regional Vp/Vs values identified by Andinisari et al. (2021a).

Some of the stations were associated with considerable misfits in the calculated versus observed travel times, that are related to site effects not captured by the 3D velocity model. To stabilize the location solutions we estimated station terms by performing a repeated location for selected events that have an azimuthal gap with no observations smaller than 180° and include more than 20 phase onset picks. This subset of earthquakes was located repeatedly. Average residuals after each iteration served as input station correction terms for the consecutive iteration. After five iterations, the average residuals no longer decreased compared to the previous iteration and the station correction terms were used for the final location of all events. Final station correction terms, up to 0.4 s, are presented in Supplements Figure S2.

3.4 Determination of Mw Magnitudes

We used the method of Ottemöller and Havskov (2003) to determine Mw moment magnitudes by the analysis of source spectra. This method searches iteratively for an optimal combination of the seismic moment (M_0) and corner frequency to fit the observed displacement spectrum. We used two different types of input data, vertical component data for land stations and hydrophone data for ocean bottom. The use of the hydrophone channel instead of the vertical channel for the ocean bottom station is justified by the following reasons. (i) A previous ocean bottom experiment (Tilmann et al., 2008) showed that the hydrophone has a higher sensitivity at frequencies below ~ 1.0 Hz compared to the operated seismometers und thus the viable range of frequencies available for magnitude determination is larger when using the hydrophone instead of the vertical channel. (ii) We calculated Mw magnitude for the OBS stations from both, the vertical seismometer channel and the hydrophone. However, the magnitude determination from the vertical channel failed for a larger number of events than from the hydrophone. (iii) In addition, absolute magnitude values determined for single events show less variation when we used the hydrophone instead of the vertical channel. We took the following approach when using the hydrophone channel for Mw determination. The instrument response was removed from the raw data and the trace was multiplied with a sound velocity of 1.5 km/s and the density of water. The resulting signal represents an approximation of the vertical displacement at the seafloor for a vertically incident ray and a negligible impedance contrast at the seafloor. This approach is supported by the fact that seafloor sediments are highly porous volcanic sediments (Cantner et al., 2014) and seismic phases arrive at near vertical angle at the ocean bottom stations. In Supplements Figure S3a, we compare the Mw magnitudes of individual earthquakes calculated from the hydrophone channels of ocean bottom stations against Mw values calculated from vertical channels of land stations. Both Mw magnitudes are in good agreement.

3.5 Re-location of Hypocenters using HypoDD

For earthquakes in close proximity that have similar source mechanisms and produce similar waveforms at the recording stations relative location techniques can significantly improve the location accuracy (Waldhauser and Ellsworth, 2000). To re-locate the earthquakes in the Kolumbo region we use the HypoDD software (Waldhauser, 2001) and two types of input data. First, we use differential traveltimes calculated from the manually picked phase arrivals and second we use differential traveltimes calculated from cross-correlation of waveforms. The cross-correlation of waveforms was performed by using the vertical channel of land stations and the hydrophone channel of ocean bottom stations. For the cross-correlation we used a 2.0 seconds window around the arrival pick and included all arrivals with a correlation coefficient > 0.75 on at least four stations.

Since the relative location method is less affected by deviations in the seismic velocity structure than absolute location approaches (Waldhauser and Ellsworth, 2000) we used a 1D velocity model for the hypocenter relocation with HypoDD. This 1D model was extracted from the 3D model of Heath et al. (2019) in the Anydros Basin. For relocating the entire earthquake dataset we used the conjugate gradients method (Paige and Saunders, 1982) which is adequate for large datasets but likely underestimates the location errors (Waldhauser and Ellsworth, 2000). The re-location yielded a dataset of 2360 events with an average traveltime residual of 0.02 ± 0.01 s. The average relative location uncertainties for the HypoDD relocated hypocentres are 0.06 ± 0.03 km in the E-W direction, 0.04 ± 0.03 km in the N-S direction and 0.04 ± 0.03 km in the vertical direction. Histograms of the uncertainties are included in the Supplements Figure S5 and Supplements Figure S6 illustrates the shift in hypocenter location between the NonLinLoc and HypoDD solutions of individual events.

3.6 Inversion of Moment Tensors

We computed full Moment Tensor solutions (MTs) for the largest events with magnitudes above Mw 2.7 using the probabilistic full waveform inversion tool *Grond* (Heimann et al., 2018; Kühn et al., 2020). As input data, we combine the vertical component records of close-by OBS stations with vertical and transversal component records of land stations (distance <50 km). Full waveforms and amplitude spectra of the land stations are fitted in frequency ranges between 0.2 and 0.6 Hz. Time window lengths range from ~10 to 20 s depending on the event-station distance, starting with manually picked P onset times until the theoretical arrival of a wave with v=2.5 km/s. The instrument transfer functions of the OBS stations are less precisely known, leading to offsets of absolute amplitudes. Therefore, we use a maximum cross-correlation fitting approach instead of the standard time-domain sample-wise fitting and the amplitude spectra fitting (see also Petersen et al., 2021). Synthetic data is forward modelled using a pre-calculated Green's function database, created from a 1D Vp model that has been calculated by averaging the 3D Vp model of Heath et al. (2019) in the region of Kolumbo. Green's functions were calculated using the *qseis* code from Wang (1999) which is implemented in the *fomosto* software (Heimann et al., 2019). The inversions for each earthquake was performed in 101 independent bootstrap chains with different random weightings of the station-component-based misfits. The ten best MT solutions of each bootstrap chain, all together 1010 solutions, were used to analyse the uncertainties of the best solution.

4. Results

4.1 Spatial Distribution of Seismicity below Kolumbo

The event location procedure with NonLinLoc based on a regional 3D Vp model yielded a dataset of 3813 earthquakes. Numerous earthquakes are outside the network or have location solutions with spurious uncertainty. To achieve a final seismicity dataset of well-located hypocentres, suitable for the later geological interpretation, we removed all events violating the following three criteria. The root-mean-square misfit of traveltimes is smaller than 0.2 s, the azimuthal gap in station coverage is smaller than 300° and the closest station recording an S phase is not further away than 1.5 times the hypocenter depth (Gomberg et al., 1990). Applying these selection criteria our final seismicity dataset contained 2803 earthquakes, which have an average root-mean-square traveltime misfit of 0.13 ± 0.03 s, an average horizontal uncertainty of 2.35 ± 1.80 km and an average vertical uncertainty of 1.3 ± 1.07 km. For events near Kolumbo the uncertainties are even smaller, due to the denser spacing of stations. Further information about location errors is included in Supplements Figure S4. The final seismicity dataset is complete for earthquakes of magnitudes above Mw ~0.5, illustrated by the frequency magnitude distribution in Supplements Figure S3c.

The strong clustering of seismicity in the crust below Kolumbo is highlighted by the fact that 2058 of the 2803 earthquakes in our final seismicity dataset are located closer than 5 km from the Kolumbo crater (Fig. 1a, 3b-c). Below Kolumbo the seismicity clusters in a cone-shaped volume, the tip of which is at ~2 km below sealevel and the base of this cone is located ~18 km below sealevel (Fig. 1c-f). In map view the cone of clustered seismicity is elongated in SW-NE direction and covers the entire Kolumbo edifice and a volcanic cone located ~2 km NE of the crater (Fig. 3).

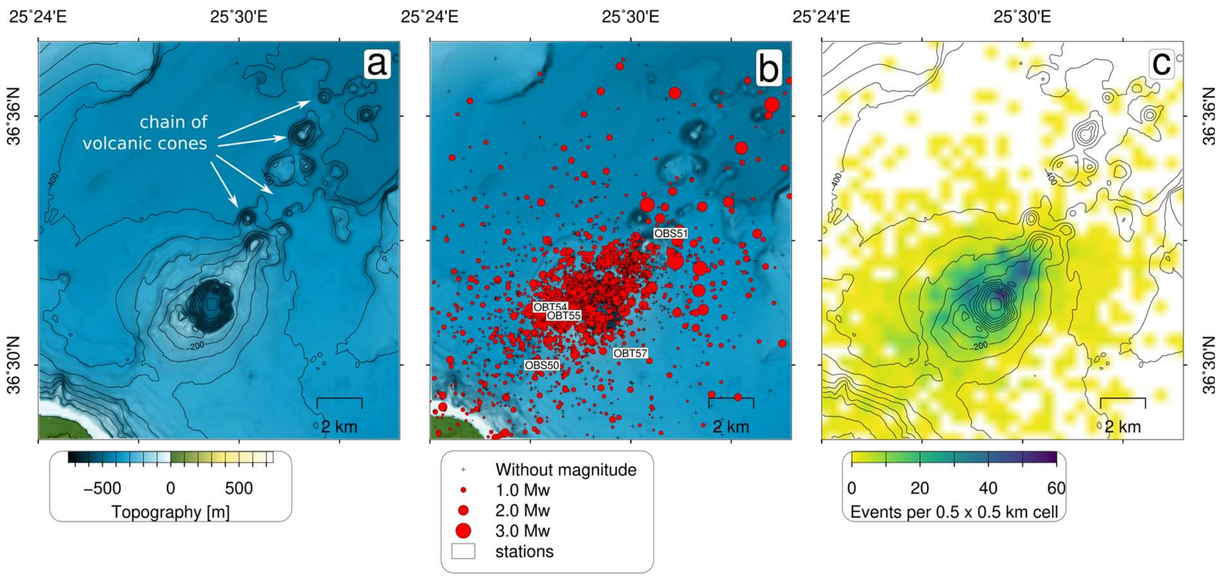

Figure 3. *a) Bathymetry of the Kolumbo crater and smaller volcanic cones NE off Kolumbo. b) Distribution of epicentres and ocean bottom stations. c) Map showing the density of epicentres.*

Comparing the vertical distributions of earthquake numbers and cumulative seismic moment release beneath Kolumbo reveals some interesting differences (Fig. 4). While the event numbers exceed 100 events per 1 km depth-bin for the interval between 4 and 10 km below sealevel, the cumulative seismic moment shows a prominent peak at 8 km below sealevel (Fig. 4). Noteworthy is that the majority of hypocentres locates at depths between 2-7 km below sealevel, but these events are of small magnitude and hardly contribute to the cumulative seismic moment release. On the contrary, stronger but fewer earthquakes occur in the depth range between 6-9 km (Fig. 4a). At 16 km a single Mw = 3.3 earthquake causes a second peak in the cumulative seismic moment distribution (Fig. 4a).

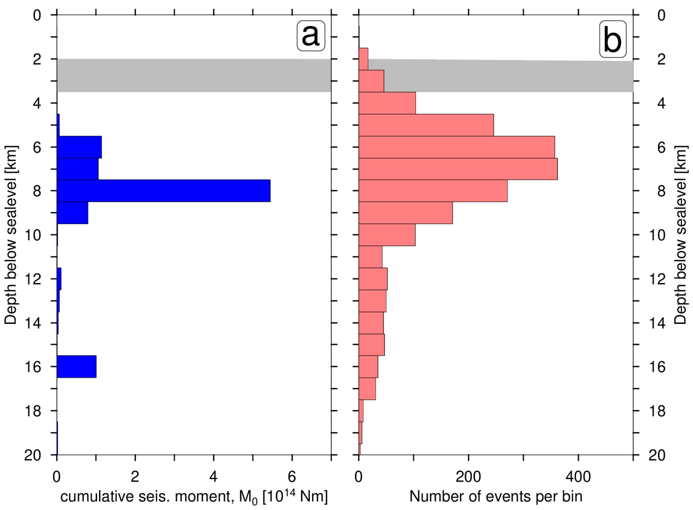

Figure 4. *a) Cumulative seismic moment release in 1 km depth bins for all events within 5 km of Kolumbo crater. b) Cumulative number of events in 1 km depth bins. The grey shading in panels a and b indicates the depth range of the shallow melt reservoir image by Chrapkiewicz et al. (in review).*

4.2 Temporal Distribution of Seismicity below Kolumbo and Earthquake Swarms

The occurrence of seismicity strongly varies over the ten month recording period. Figure 5b and 5c present hypocenter depths, magnitude and cumulative seismic moment release versus time for all earthquakes located within 5 km of the Kolumbo crater. The event rate shows strong variations over time, ranging between zero and 200 events per 24 hours. The occurrence of earthquakes with magnitudes Mw > 2.5 partly correlates with the event rate (Fig. 5b). For example, in the days marked as swarm #1 and swarm #4, Mw 2.7-3.4 earthquakes coincide with peaks in the event rate. In other instances, e.g. on the days marked as swarm #2 and swarm #3, the event rate is increased but does not coincide with stronger earthquakes. The opposite is the case in early December 2006 where two earthquakes of Mw 3.4 and Mw 3.7 occur but the event rate remains below 50 events per 24 hours (Fig. 5b).

The temporal distribution of seismicity suggests the occurrence of several earthquake swarms. In contrast to mainshock-aftershock sequences, these earthquakes swarms do not exhibit an exponential decay in the aftershock rate (e.g. Shcherbakov et al., 2004). We scanned the seismicity dataset and did not identify any typical mainshock-aftershock sequences. Instead, we consider the instances of increased event rate in the crust below Kolumbo to be earthquake swarms. In the following, we will look into the four swarms that exhibit the highest event rates (marked by black arrows, labelled as swarms #1 - #4 in Figure 5b). Besides the four earthquake swarms marked in Figure 5b our seismicity dataset includes several additional swarms. However, they include less events and show similar characteristics as the four considered swarms, so we consider the four strongest swarms as representative of the swarm activity below Kolumbo.

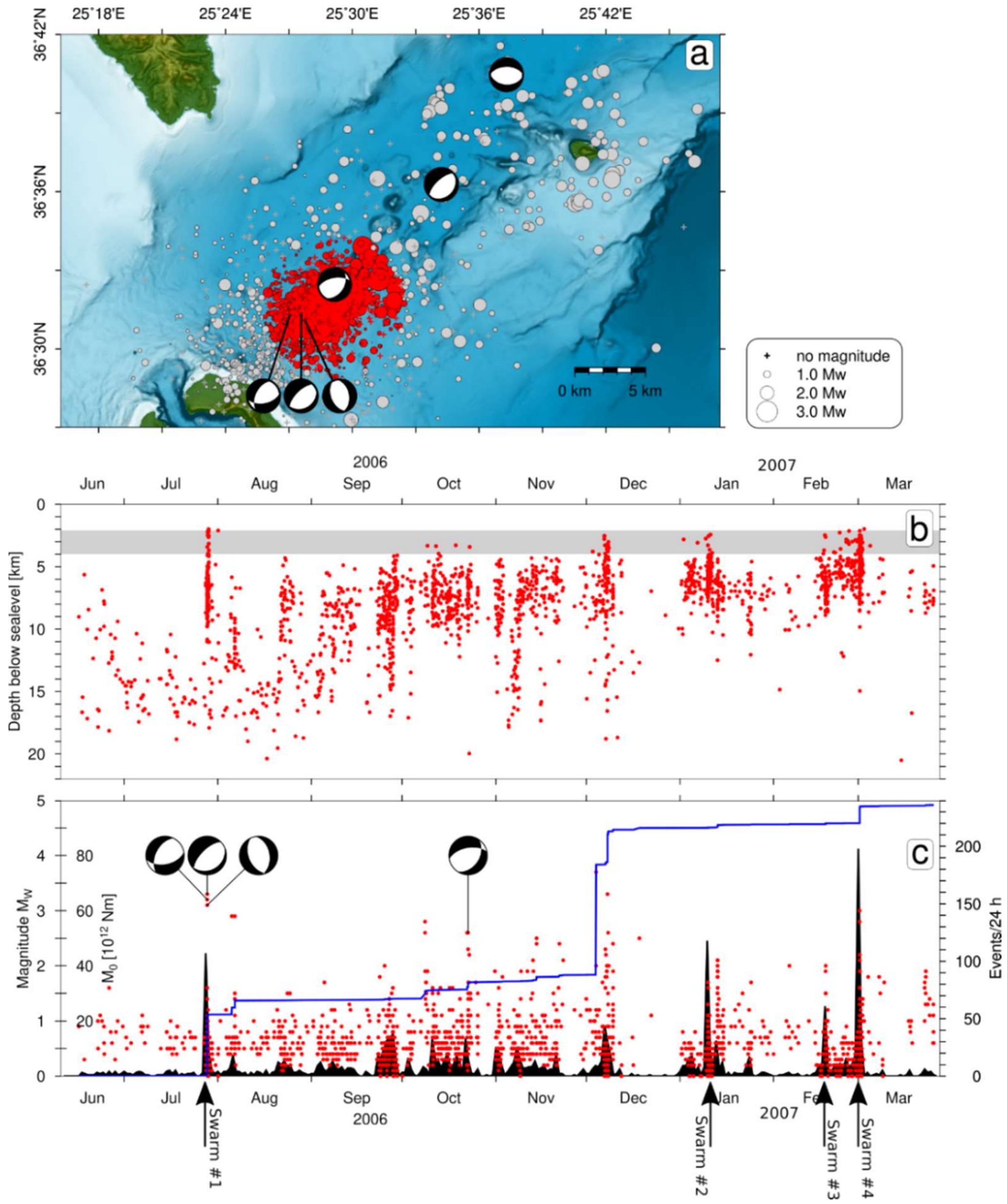

Figure 5. *a) Map with NonLinLoc located epicentres coloured according to distances closer (red) and further (grey) than 5 km from Kolumbo. Beachballs represent the double-couple components of six earthquakes yielding stable MT inversion results. Panels b and c only include earthquakes closer than 5 km from the crater. b) Hypocenter depths versus time. The grey shading indicates the depth range of the shallow melt reservoir imaged by Chrapkiewicz et al. (in review). c) Black shading indicates the event rate per 24 hours. Red dots show Mw magnitudes versus time. The blue curve shows the accumulated seismic moment, Mo, versus time. Onset times of the four seismicity swarms plotted in Figures 7 and 8 are indicated by black arrows.*

4.3 Moment tensors of Mw 2.7 – 3.7 earthquakes

We performed MT inversions for all earthquakes with Mw 2.7 and larger, in total 12 earthquakes. Following the approach described in section 3.6, we were able to obtain six stable solutions (Fig. 5 and 6; see also Supplements Fig. S8 with additional inversion parameters for an example event). All MT solutions show dominant normal faulting mechanisms (Fig. 5a). Four earthquakes show NE-SW striking fault planes that are sub-parallel to the axis of minimum regional stress (σ_3) in the crust (Konstantinou and Yeh, 2012). As often observed for small earthquakes, the non-DC components are not well resolved (e.g. Cesca et al., 2006; Panza and Saraò, 2000; Petersen et al., 2021). Low signal-to-noise ratios due to oceanic noise conditions and the relatively wide frequency range used in the full waveform inversion, which may not be adequately resolved, can influence the stability of MT solutions. Additionally, the small number of seismic stations result in spurious or not well-resolved non-DC components. For the three best-resolved earthquakes, isotropic components constitute less than 10 % of the total seismic moment, pointing at a predominantly tectonic origin of the earthquakes. We do not find a significant improvement of misfits when allowing non-DC components compared to a pure DC.

Three earthquakes with MT solutions are part of swarm #1 (Fig. 5 and 7). One earthquake with MT solution represents the strongest earthquakes of a seismicity burst below Kolumbo in October 2006 (Fig. 5b). Two events with MT solutions are located in the Anydros Basin NE off Kolumbo (Fig. 5a). For the remaining six earthquakes with Mw >= 2.7 the MT inversions did not yield stable solutions for various reasons. For two earthqukes, the waveforms are overlapping with smaller events and in the other cases, the signal-to-noise ratio in the utilized frequency range is not sufficient at a minimum of 3-4 azimuthally well-distributed stations.

347

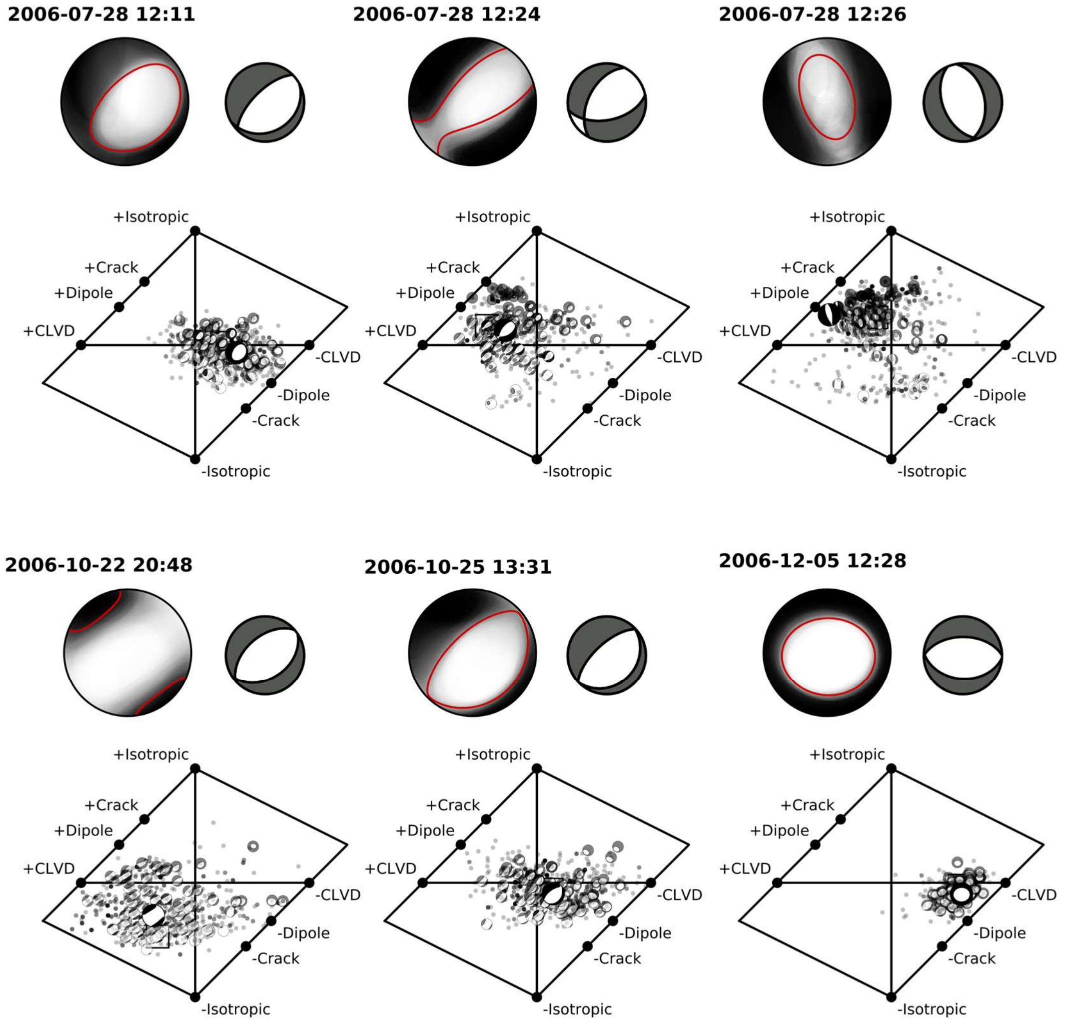

Figure 6. *Results of the moment tensor inversions for six earthquakes. For each earthquake the fuzzy beachball, the double couple component of the full moment tensor and the Hudson plot is presented. The fuzzy beachballs illustrate the uncertainty of the MT inversion. The plots represent the stacked the P-wave radiation pattern strength of every solution of the different bootstrap chains. In case of stable results, the fuzzy plot has clearly separated black and white fields. The best solution is indicated by red lines. The diamond-shaped Hudson plots show the variability of the non-DC components of the bootstrap-chain solutions. CLVD = compensated linear vector dipole.*

4.4 Characteristics of earthquake swarms

Figure 7 shows a time versus depth distribution of the four analysed swarms and Figure 8 presents the locations of swarm events after relative relocation with the HypoDD software. The durations of the four earthquake swarms range between 2.3 h (swarm #3) and 23.1 h (swarm #2). All four swarms initiate with an almost synchronous onset of several Mw 2-3 earthquakes spread-out over a depth range of ~4 km (Fig. 7). Swarms #1, #2, #4 show a distinct separation into an early phase and a later phase (Fig. 7). The early phase is characterized by stronger earthquakes at 4-9 km depth below sealevel, the later phase is characterized by weaker events (Mw < 1.5) occurring at 2-7 km depth below sealevel (Fig. 7). The initial hypocentres in each swarm (yellow stars in row a, Fig. 7) are deeper than the majority of events during the later phase of the swarms, indicating a general upwards directed trend in the migration of hypocentres in all swarms. The solid black lines in Fig. 7c shows the theoretical propagation velocity of fluids that have a pressure source near the location of the initial hypocenter and have a diffusivity of 300 and 100 m^2/s, calculated according to the equation $r = \sqrt{4\pi Dt}$ from Shapiro et al. (1997). In this equation r is distance from the pressure source (hypocenter of the initial swarm earthquake), t is time and D is hydraulic diffusivity. For swarms #1, #3, #4 the propagation of the cracking front corresponds to a theoretical fluid diffusivity of 1000 m^2/s and for swarm #2 the propagation to fluid diffusivity of 300 m^2/s.

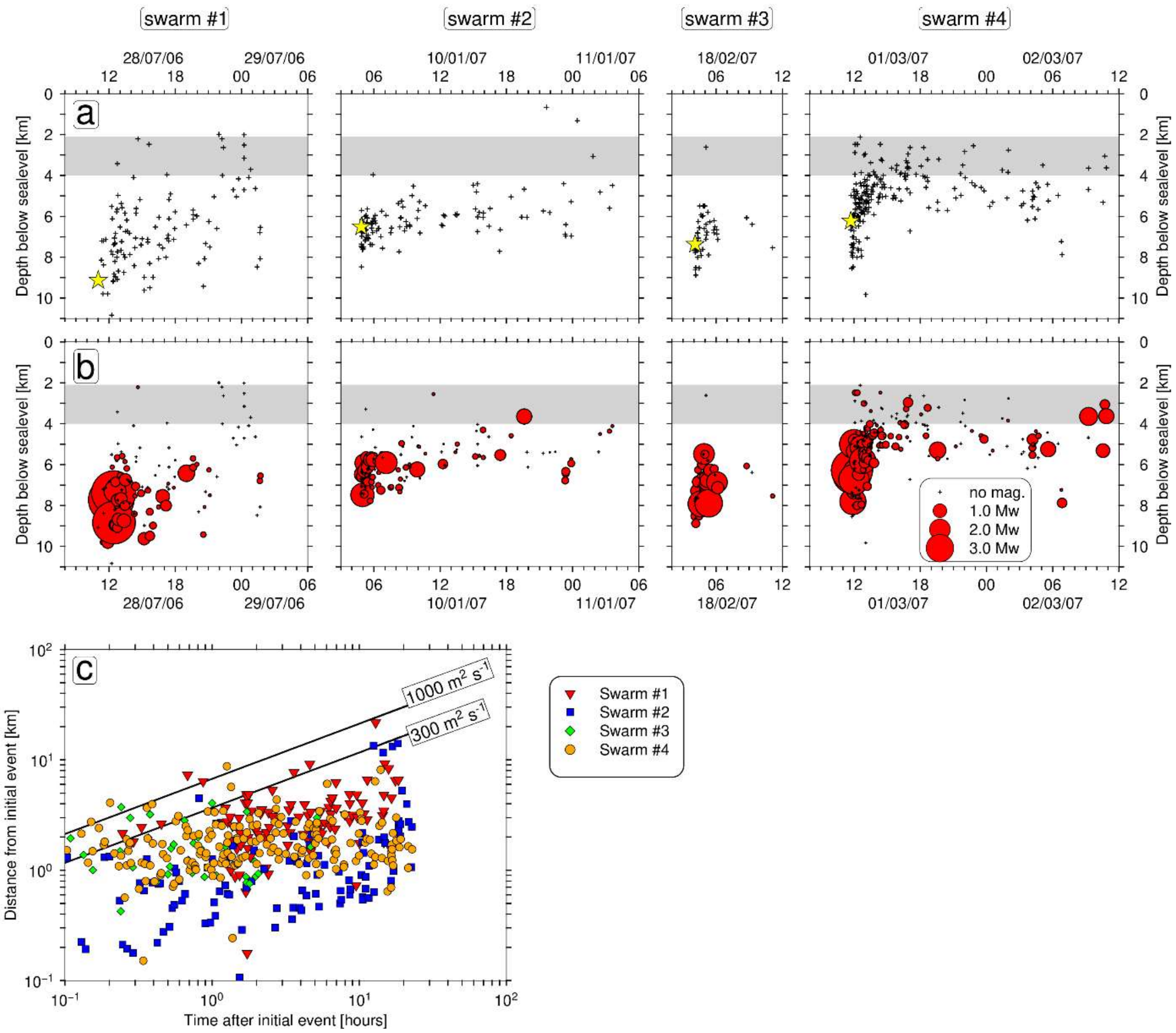

Figure 7. *Row a, time versus depth distribution of events in the four earthquake swarms analysed. Yellow stars in row a indicate the depths of initial hypocentres in each swarm. Panels in row b are identical with row a, but include magnitudes. The grey shading in rows a and b indicates the depth of the shallow melt reservoir imaged by Chrapkiewicz et al (in review). c) Log-log plot showing the propagation of hypocentres in individual swarms relative to the initial hypocenter of each swarm. The two solid black lines indicate theoretical hydraulic diffusivities of 300 and 1000 m²/s in a fault zone, emanating from a point source.*

Despite the improved relative location accuracy of hypocentres after re-location with the HypoDD software, the four swarms do not collapse in a single location but occupy different volumes of the crust below Kolumbo (Fig. 8). In particular, the map view with epicentres (Fig. 8a) and the cross-section striking from SW to NE (Fig. 8b) demonstrate that the four swarms represent brittle fracturing in nearby, yet different volumes of the crust. Except for swarm #1 all swarms show a larger spatial extent in the vertical domain than in the horizontal domain (Fig. 8).

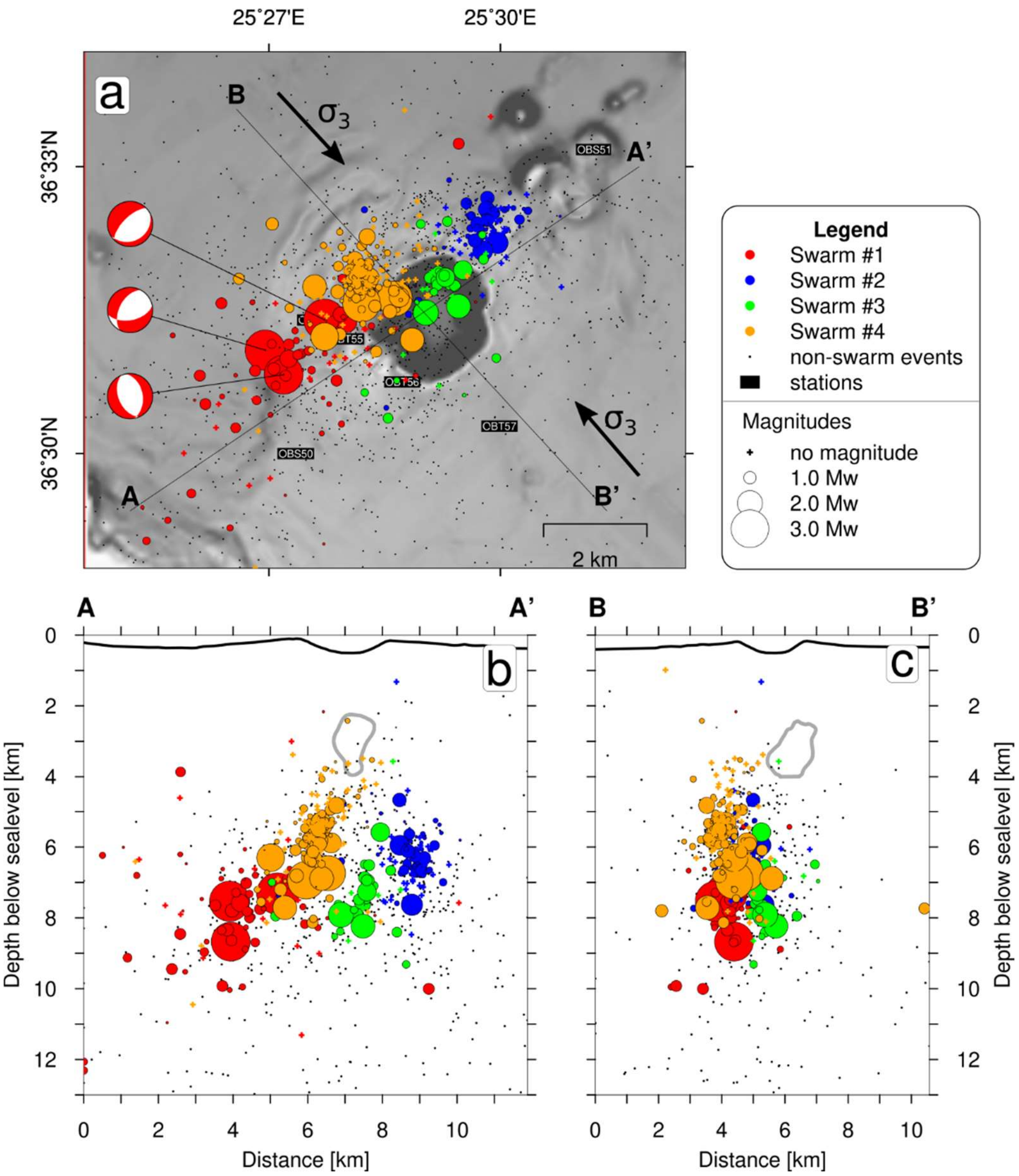

Figure 8. *Epicentres and hypocentres of swarm earthquakes after relative re-location with the HypoDD software. Colours represent the four earthquake swarms presented in Fig. 7. The solid black arrows indicate the principal axis of least compressive stress (σ₃) from Dimitriadis et al. (2009). The polygons encircled by a solid grey line in panels b and c indicated the position of a shallow crustal melt reservoir imaged by Chrapkiewicz et al. (in review). Note, the vertical and horizontal scales are identical in panels b and c. Panel a is slightly enlarged.*

The seismograms of swarm events show strong spectral power in the 5-15 Hz frequency range, illustrated by the waveforms and spectrograms of an earthquake from swarm #1 (Fig. 9). Such a dominance of frequencies above 5 Hz is typical for volcano-tectonic (VT) events according to the widely-used classification of volcanic seismicity (Lahr et al., 1994).

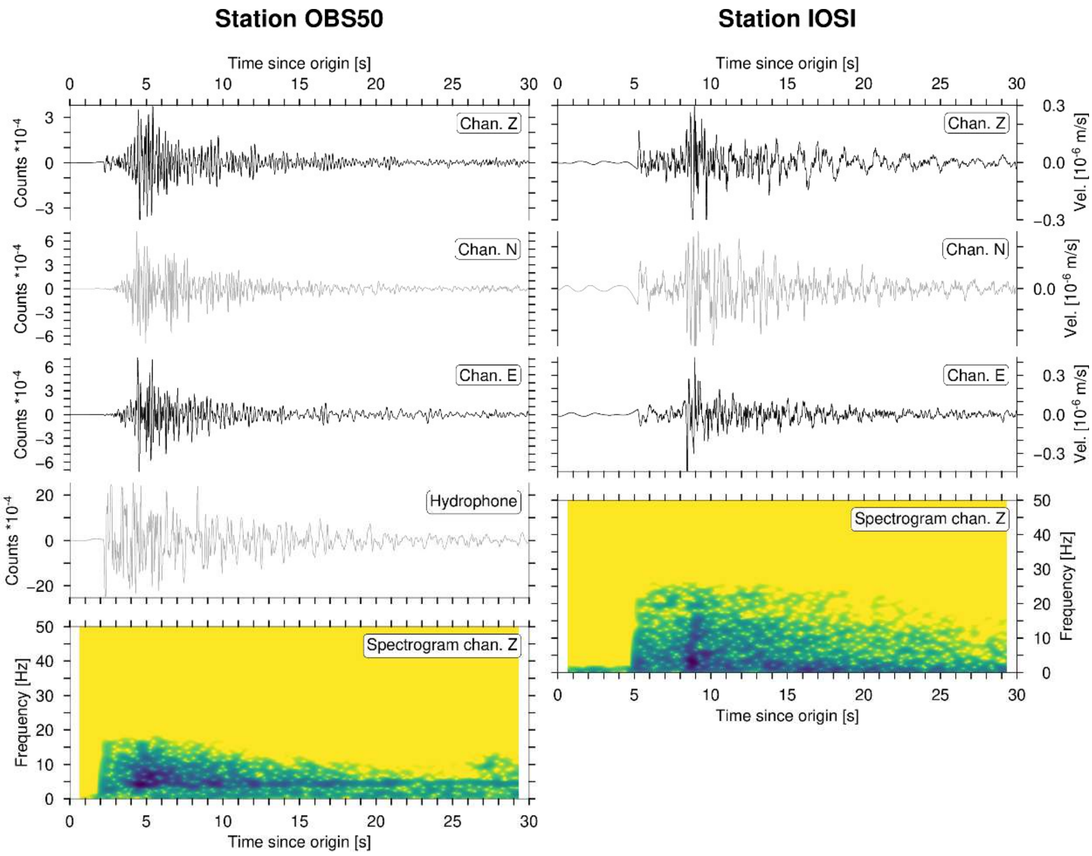

Figure 9. Waveform examples of an Mw 3.1 earthquake at 7.8 km depth below Kolumbo occurring in swarm #1. The origin time is 2006-07-28 12:11:14. Left hand panels show seismograms and spectrogram for stations OBS50. Right hand panels show seismograms and spectrogram for station IOSI. Darker colours in the spectrograms correspond to increased spectral power; lighter colours correspond to decreased spectral power.

5 Discussion

Our dense network of stations near Kolumbo produced a seismicity dataset of low-magnitude events with high location accuracies that allow us to understand the processes controlling the fine-structure of seismic faulting beneath Kolumbo at unprecedented detail in space and time.

5.1 Relation of seismicity with crustal P-wave velocity structure and partial melt region

The tip of the cone-shaped seismically active volume below Kolumbo coincides with a prominent anomaly of strongly reduced Vp, ~1.5 km/s slower than the regional average (Fig. 10). This anomaly was imaged through full-waveform inversion of active source seismic data acquired in 2015 by the PROTEUS experiment and is interpreted as a body of 28-44% percent partial melt and has an approximate size of 6 km^3 (Chrapkiewicz et al., in review). A few earthquakes locate inside this volume but their seismograms have weak signal amplitudes, preventing magnitude determination (Fig. 10). It should be noted that the active seismic survey was conducted about nine years after our deployment and the size of the crustal melt reservoir may have changed in the meantime.

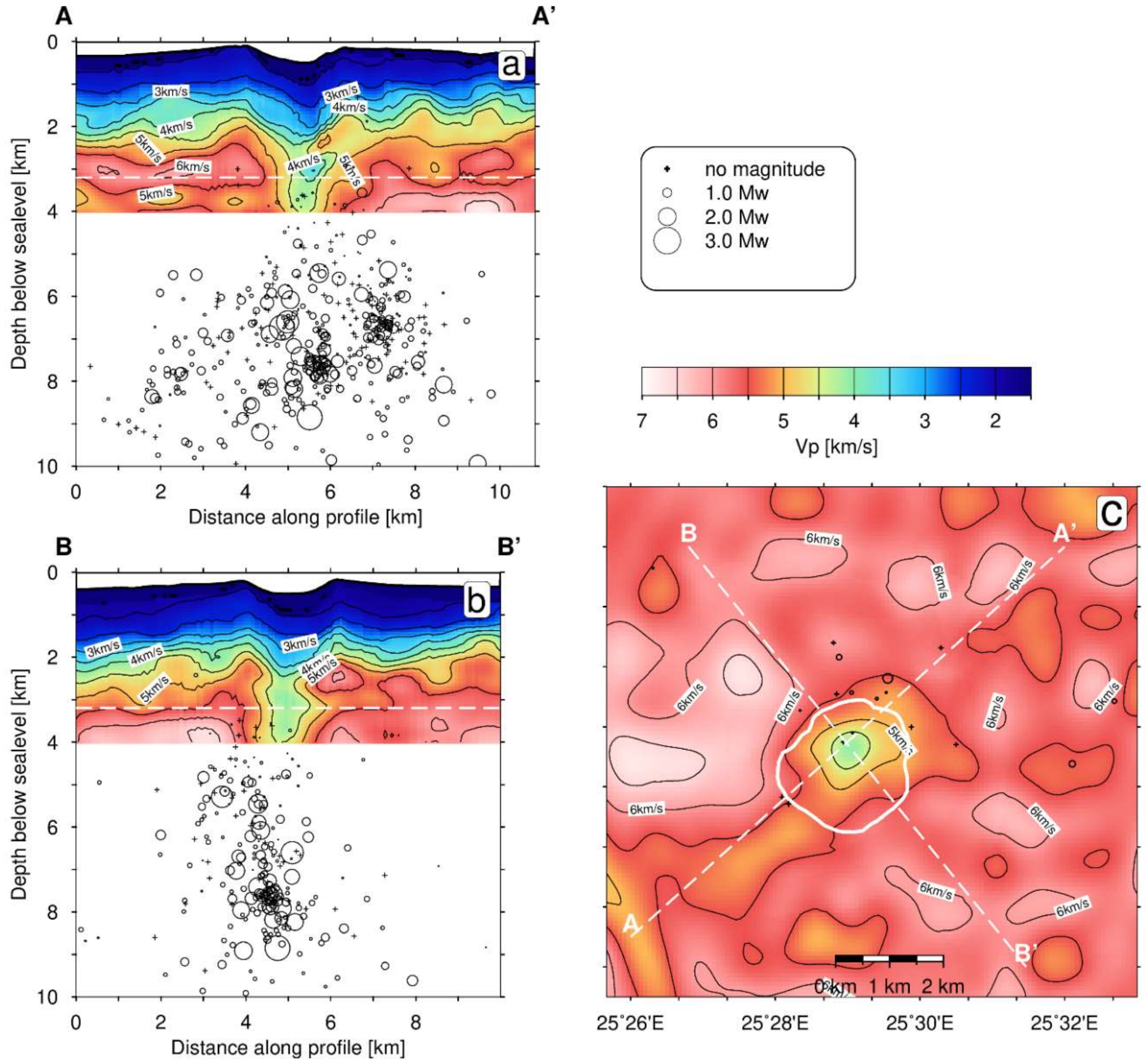

Figure 10. *3D P wave velocity structure and microseismicity beneath Kolumbo. Panels a and b show cross-sections through the 3D Vp model of Chrapkiewicz et al. (in review) with contour lines spaced at 0.5 km/s and hypocentres of this study superposed. Dashed white lines in panels a and b indicate the depth of panel c. Note, this 3D tomography model terminates at 4 km depth. c) Depth slice at 3.2 km depth below sealevel. Dashed white lines indicate the locations of panels a and b. The solid white line indicates the location of the crater rim. Epicentres are plotted for all earthquakes between 2.7-3.7 km depth below sealevel. Note, a region with Vp reduced by 1.0-1.5 km/s between 2.1-4.0 km depth immediately below the Kolumbo crater, interpreted as a crustal melt (Chrapkiewicz et al., in review).*

Combining all observations derived from the analysis of our earthquake dataset and other geophysical datasets of the Kolumbo region, we find that both regional tectonics and fluids in the crust have a significant influence on the seismic activity in this region. Below, we first separately discuss these relations and then establish a combined interpretation of co-seismic processes in the crust below Kolumbo including potential changes during the recent two decades.

5.2 Relations of earthquake swarms and regional tectonics

All six achieved MT solutions indicate normal faulting (Figs. 5, 6), in agreement with previously presented focal mechanisms for this region (Andinisari et al., 2021b; Dimitriadis et al., 2009). The region of seismic swarm activity is elongated in SW-NE direction parallel to the strike direction in four out of six focal mechanisms (Fig. 5, 8) and perpendicular to the principal axis of least compressive stress (σ_3; Fig. 8; Dimitriadis et al., 2009). We suggest that the swarm seismicity is associated with a SW-NE oriented zone of fractures aligned parallel to the trend of regional faults and basins of the Santorini-Amorgos extensional tectonic zone (Fig. 1; Heath et al., 2019; Hooft et al., 2017; Sakellariou et al., 2017). The swarm earthquakes are of volcano-tectonic character with strong spectral power above 5 Hz (Fig. 9) and the moment tensors indicate a minor non-DC component, which suggests that the co-seismic faulting in this zone of fractures is influenced by the regional extensional tectonics.

Heath et al. (2021) investigated the orientations of local-scale faults/fractures in the study area by means of anisotropic active-source traveltime tomography, based on the PROTEUS experiment conducted in 2015 (Hooft et al., 2019). The results of Heath et al. (2021) yield low seismic anisotropy (< 5 %) in the Kolumbo region and they conclude that magmatic processes in the Santorini-Kolumbo region are strongly influenced by regional-scale, but hardly influenced by local-scale processes. This dominance of regional-scale tectonic processes agrees with the faulting mechanism and spatial distribution of earthquakes in our dataset (Fig. 5, 6).

5.3 Relations of earthquake swarms and fluids

Earthquake swarms are typical in active volcanic systems and commonly interpreted in association with fluid-related processes (e.g. Duputel et al., 2019; Hensch et al., 2008; Shelly et al., 2013; Tarasewicz et al., 2012; Yukutake et al., 2011). An increase in fluid pressure, intruding magma or aseismic slip are feasible processes that locally increase the shear stress and/or reduce the effective normal stress and thereby trigger earthquake swarms (Shelly et al., 2013; Vidale and Shearer, 2006; Yukutake et al., 2011). At Kolumbo the presence of fluids is documented independently from seismicity by vigorously venting hydrothermal chimneys inside the crater (Carey et al., 2013; Rizzo et al., 2019) and the identification of a crustal melt reservoir below the crater (Fig. 10; Chrapkiewicz et al., in review). Geochemical analyses of fluids vented inside the Kolumbo crater suggest that the root of the hydrothermal system is located at ~1 km depth below sealevel (see cartoon in Fig. 11; Rizzo et al., 2019). At this depth, ascending volcanic gases mix with cold seawater and consecutively ascend to the seafloor (Rizzo et al., 2019). The crustal melt reservoir lies beneath the mixing level at 2.1-4.0 km depth (Figs. 10, 11) and releases the volcanic gases feeding the hydrothermal system (Fig. 11). Previous studies hypothesized a steady replenishment of this melt reservoir with mafic melts ascending from the mantle and infer this processes is linked to the persistent seismic unrest beneath Kolumbo (Andinisari et al., 2021a; Klaver et al., 2016; Konstantinou, 2020). We endorse this hypothesis and add further detail to it in the following paragraphs.

We assume that the crust below Kolumbo is saturated with fluids and beneath the melt reservoir, the fluids are most likely melts. We further hypothesize that the observed swarm seismicity was, at least partially triggered by perturbations in pore-fluid pressure. For such triggering, several mechanism have been proposed including hydraulic fracturing, pore pressure relaxation, the redistribution of elastic stresses or a combination of these mechanisms (Hainzl, 2004; Maillot et al., 1999; Shapiro et al., 1997; Shapiro et al., 2003). Several studies identified swarm seismicity in volcanically and hydrothermally active regions where the propagation of the co-seismic cracking front corresponds to predicted fluid diffusion in the subsurface with hydraulic diffusivities of about 1.0 m^2/s (e.g. Shelly et al., 2013; Yukutake et al., 2011). In all four analysed swarms, the cracking front shows a constant upwards propagation, which would correspond to fluids with a hydraulic diffusivity of 300-1000 m^2/s (Fig. 7c). However, this propagation rate is significantly faster than the typical range of fluid diffusivities (0.2-300 m^2/s) inferred from the cracking front propagation velocities in previous studies (Shapiro et al., 1997; Shapiro et al., 2003; Shelly et al., 2013; Yukutake et al., 2011).

The fast propagation of the cracking front in the four analysed earthquake swarms suggests that a direct relation to diffusing fluids injected at a point source and hydraulic fracturing as sole triggering mechanism is unlikely. A direct relation of the swarm seismicity with the propagating tip of a dike seems unlikely as well. Seismicity linked to laterally propagating dike tips is typically in the range 0.05-0.38 m/s (e.g. Dziak et al., 2007; Sigmundsson et al., 2015). For vertically ascending dikes the propagation varies as a function of depth and may reach values up to 3.05 m/s only close to the surface (Battaglia and Bachèlery, 2003; Rivalta and Dahm, 2006) which is slower than the hypocentre propagation we observed (Fig. 7c).

Considering the upwards migration of hypocentres during all four analysed swarms (Fig. 7a) and the fast propagation of the cracking front (Fig. 7c) we propose that a combination of pore-pressure perturbations and the re-distribution of elastic stresses is a more likely triggering mechanism of the swarm seismicity. We infer that several, near-vertical melt conduits already existed during the period of our experiment and the four earthquake swarms correspond to the locations of those conduits (Fig. 6). Analogue modelling by Kavanagh et al. (2018) showed that fluids in a vertically ascending dike can move significantly faster than the dike tip itself, explaining the fast propagation of the co-seismic cracking front in the swarms.

The initial hypocentres in all four swarms (yellow stars in Fig. 7a), the strongest earthquakes and the highest cumulative moment release occur in the depth range between 6 and 9 km below sealevel (Fig. 4a). We propose that the ascend of melts coming from the mantle is obstructed in the region between 6-9 km depth by a rheologically strong layer (Fig. 11) and some kind of bottlenecks or solidified melt plugs may be present in this depth range. Those structures may occasionally perturbing or hamper the flow inside the melt conduits, as previously suggested by Tarasewicz et al. (2012). Transients in the fluid pressure could also be induced by dynamic triggering from purely tectonic local or regional earthquakes (e.g. Aiken and Peng, 2014; Cattania et al., 2017), which is supported by the strong relation of seismicity and regional tectonics (section 5.2).

The co-seismic tensile faulting creates an approximately 3 km wide zone of fractures in the crust below Kolumbo (Fig. 11) and this zone is exploited by ascending melts, probably throughout the recent decades as indicated by the persistent seismic unrest (Fig. 2). During the year 2021, the seismic unrest has increased (Fig. 2), which can be interpreted as indication of an increase in magmatic activity. In the light of still ongoing seismic unrest (Fig. 2) and the presence of a crustal melt reservoir (Fig. 10) our findings suggest that the melt plumbing system below Kolumbo is highly active, and a significant risk of future eruptions exists. It is beyond the scope of this study to quantify the melt flux from the mantle into the shallow melt reservoir but our results demonstrate that close monitoring of Kolumbo is advisable to keep on top of any volcanic hazards and minimize the risk for the nearby communities.

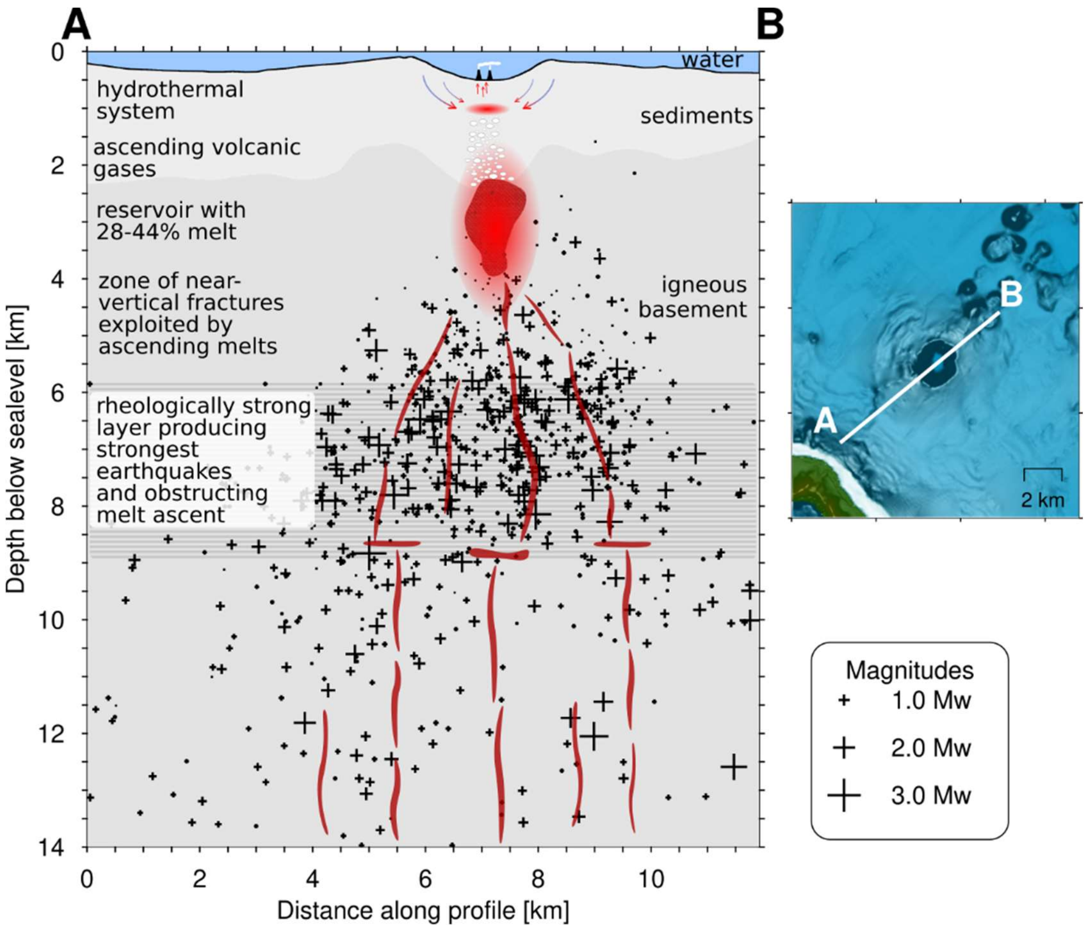

Figure 11. *Interpretation cartoon illustrating the melt-plumbing system and on-going tectono-magmatic-hydrothermal processes below Kolumbo. Map to the right indicates the location of cross-section. Black crosses show projected NonLinLoc located hypocentres scaling with magnitude. The location of the melt reservoir is from Chrapkiewiz et al. (in review).*

6 Conclusions

This study presents a ten-month long dataset of microseismicity around the submarine Kolumbo volcano in the southern Aegean that is a focal point of recurring seismic unrest, lasting since at least two decades. Our final seismicity dataset contains 2803 earthquakes with magnitudes of 0-3.7 Mw. The majority of the epicentres (2058) are located within 5 km of Kolumbo crater where they cluster in a cone-shaped volume located between 2 and 18 km below sealevel.

We captured several earthquake swarms beneath Kolumbo, of which the four strongest ones were analysed in detail. The four swarms occupy nearby, yet different volumes of the crust indicating that they are not associated with a single fault. Instead, the region of swarm seismicity is elongated in SW-NE direction, parallel to the orientation of regional faults and perpendicular to the principal axis of least compressive stress. The relation of swarm seismicity with regional extension tectonics is further demonstrated by six determined moment tensors showing exclusively normal faulting mechanisms.

All four swarms initiate with an almost synchronous onset of Mw 2.0-3.0 earthquakes at 5-9 km depth and in the later phase of each swarm the earthquakes become shallower and weaker. The fast propagation of the cracking front in the four analysed swarms (300-1000 m^2/s) suggests that a triggering by hydraulic fracturing from fluids injected at a point source or active diking is unlikely. We conclude that the swarm seismicity in 2006-2007 below Kolumbo was more likely triggered by a combination of fluid-pressure perturbations and the redistribution of regional stresses. The perturbations in the fluid pressure may either be induced by obstructions in the melt flow in a rheologically strong layer between 6-9 km depth or via dynamic triggering of purely tectonic local or regional earthquakes.

Active seismic imaging of the crust below Kolumbo in 2015 revealed a ~6 km^3 large reservoir of 28-44% melt that is located at 2.1-4.0 km depth below sealevel. The location of this melt reservoir coincides with the tip of the cone-shaped seismically active region and we conclude that the observed swarm seismicity in 2006-2007 contributed to the creation of a zone of fractures in the crust below Kolumbo that are later exploited by ascending melts feeding the melt reservoir. Routine earthquake monitoring based on land stations indicates that the seismic unrest below Kolumbo persisted throughout the recent two decades and has increased during the year 2021. Considering our findings derived from the swarm seismicity below Kolumbo we conclude that a conceivable risk of future eruptions exists and close monitoring of this volcanic system is advisable to minimize the associated hazards for the nearby communities.

Acknowledgements

FS was funded by a Walter Benjamin fellowship of Deutsche Forschungsgemeinschaft (DFG, grant SCHM 3522/2-1) and by GEOMAR. The operation the ocean bottom stations was funded through DFG project 19882590 (PI T. Dahm). GP was funded by DFG project 362440331. We acknowledge the crews of RV Poseidon cruises POS337, POS338 and the RV Aegaeo deploying and retrieving the instruments. We thank I. Grevemeyer for passing on the seismic dataset and for helpful comments.

Data Availability

EGELADOS seismic data are available from http://eida.gfz-postdam.de/webdc3 by searching for the network code Z3. Ocean bottom station data will be released in the www.pangaea.de archive prior to acceptance of the paper.

References

Aiken, C., and Z. Peng (2014), Dynamic triggering of microearthquakes in three geothermal/volcanic regions of California, Journal of Geophysical Research: Solid Earth, 119(9), 6992-7009, doi: 10.1002/2014JB011218.

Andinisari, R., K. I. Konstantinou, and P. Ranjan (2021a), Seismicity along the Santorini-Amorgos zone and its relationship with active tectonics and fluid distribution, Physics of the Earth and Planetary Interiors, 312, 106660, doi: 10.1016/j.pepi.2021.106660.

Andinisari, R., K. I. Konstantinou, and P. Ranjan (2021b), Moment tensor inversion of microearthquakes along the Santorini-Amorgos zone: Tensile faulting and emerging volcanism in an extensional setting, Journal of Volcanology and Geothermal Research, 420, 107394, doi: 10.1016/j.jvolgeores.2021.107394.

Battaglia, J., and P. Bachèlery (2003), Dynamic dyke propagation deduced from tilt variations preceding the March 9, 1998, eruption of the Piton de la Fournaise volcano, Journal of Volcanology and Geothermal Research, 120(3), 289-310, doi: 10.1016/S0377-0273(02)00410-9.

Bohnhoff, M., M. Rische, T. Meier, D. Becker, G. Stavrakakis, and H. P. Harjes (2006), Microseismic activity in the Hellenic Volcanic Arc, Greece, with emphasis on the seismotectonic setting of the Santorini-Amorgos zone, Tectonophysics, 423(1-4), 17-33, doi: 10.1016/j.tecto.2006.03.024.

Cantner, K., S. Carey, and P. Nomikou (2014), Integrated volcanologic and petrologic analysis of the 1650AD eruption of Kolumbo submarine volcano, Greece, Journal of Volcanology and Geothermal Research, 269, 28-43, doi: 10.1016/j.jvolgeores.2013.10.004.

Carey, S., P. Nomikou, K. C. Bell, M. Lilley, J. E. Lupton, C. Roman, E. Stathopoulou, K. Bejelou, and R. Ballard (2013), Co2 degassing from hydrothermal vents at kolumbo submarine volcano, greece, and the accumulation of acidic crater water, Geology, 41(9), 1035-1038, doi: 10.1130/G34286.1.

Cattania, C., J. J. McGuire, and J. A. Collins (2017), Dynamic triggering and earthquake swarms on East Pacific Rise transform faults, Geophysical Research Letters, 44(2), 702-710, doi: 10.1002/2016GL070857.

Cesca, S., E. Buforn, and T. Dahm (2006), Amplitude spectra moment tensor inversion of shallow earthquakes in Spain, Geophysical Journal International, 166(2), 839-854, doi: 10.1111/j.1365-246X.2006.03073.x.

Colgate, S. A., and T. Sigurgeirsson (1973), Dynamic Mixing of Water and Lava, Nature, 244(5418), 552-555, doi: 10.1038/244552a0.

Dimitriadis, I., C. Papazachos, D. Panagiotopoulos, P. Hatzidimitriou, M. Bohnhoff, M. Rische, and T. Meier (2010), P and S velocity structures of the Santorini-Coloumbo volcanic system (Aegean Sea, Greece) obtained by non-linear inversion of travel times and its tectonic implications, Journal of Volcanology and Geothermal Research, 195(1), 13-30, doi: 10.1016/j.jvolgeores.2010.05.013.

Dimitriadis, I., E. Karagianni, D. Panagiotopoulos, C. Papazachos, P. Hatzidimitriou, M. Bohnhoff, M. Rische, and T. Meier (2009), Seismicity and active tectonics at Coloumbo Reef (Aegean Sea, Greece): Monitoring an active volcano at Santorini Volcanic Center using a temporary seismic network, Tectonophysics, 465(1), 136-149, doi: 10.1016/j.tecto.2008.11.005.

Druitt, T. H., F. W. McCoy, and G. E. Vougioukalakis (2019), The Late Bronze Age Eruption of Santorini Volcano and Its Impact on the Ancient Mediterranean World, Elements, 15(3), 185-190, doi: 10.2138/gselements.15.3.185.

Duputel, Z., O. Lengliné, and V. Ferrazzini (2019), Constraining Spatiotemporal Characteristics of Magma Migration at Piton De La Fournaise Volcano From Pre-eruptive Seismicity, Geophysical Research Letters, 46(1), 119-127, doi: 10.1029/2018GL080895.

Dziak, R. P., D. R. Bohnenstiehl, J. P. Cowen, E. T. Baker, K. H. Rubin, J. H. Haxel, and M. J. Fowler (2007), Rapid dike emplacement leads to eruptions and hydrothermal plume release during seafloor spreading events, Geology, 35(7), 579-582, doi: 10.1130/G23476A.1.

Fouqué, F. (1879), Santorin et ses éruptions, par F. Fouqué, G. Masson, Paris.

Francalanci, L., G. E. Vougioukalakis, G. Perini, and P. Manetti (2005), A West-East Traverse along the magmatism of the south Aegean volcanic arc in the light of volcanological, chemical and isotope data, in Developments in Volcanology, edited by M. Fytikas and G. E. Vougioukalakis, pp. 65-111, Elsevier.

Friederich, W., and T. Meier (2008), Temporary Seismic Broadband Network Acquired Data on Hellenic Subduction Zone, Eos, Transactions American Geophysical Union, 89(40), 378-378, doi: 10.1029/2008EO400002.

Gomberg, J. S., K. M. Shedlock, and S. W. Roecker (1990), The effect of S-wave arrival times on the accuracy of hypocenter estimation, Bulletin - Seismological Society of America, 80(6 A), 1605-1628.

Hainzl, S. (2004), Seismicity patterns of earthquake swarms due to fluid intrusion and stress triggering, Geophysical Journal International, 159(3), 1090-1096, doi: 10.1111/j.1365-246X.2004.02463.x.

Havskov, J., and L. Ottemoeller (1999), SeisAn Earthquake analysis Software, Seismological Res. Lett., 70, 532-534, doi: 10.1785/gssrl.70.5.532.

Heath, B. A., E. E. E. Hooft, D. R. Toomey, M. Paulatto, C. B. Papazachos, P. Nomikou, and J. V. Morgan (2021), Relationship Between Active Faulting/Fracturing and Magmatism Around Santorini: Seismic Anisotropy From an Active Source Tomography Experiment, Journal of Geophysical Research: Solid Earth, 126(8), e2021JB021898, doi: 10.1029/2021JB021898.

Heath, B. A., E. E. E. Hooft, D. R. Toomey, C. B. Papazachos, P. Nomikou, M. Paulatto, J. V. Morgan, and M. R. Warner (2019), Tectonism and Its Relation to Magmatism Around Santorini Volcano From Upper Crustal P Wave Velocity, Journal of Geophysical Research: Solid Earth, 610-629, doi: 10.1029/2019JB017699.

Heimann, S., H. Vasyura-Bathke, H. Sudhaus, M. P. Isken, M. Kriegerowski, A. Steinberg, and T. Dahm (2019), A Python framework for efficient use of pre-computed Green's functions in seismological and other physical forward and inverse source problems, Solid Earth, 10(6), 1921-1935, doi: 10.5194/se-10-1921-2019.

Heimann, S., M. Isken, D. Kühn, H. Sudhaus, A. Steinberg, S. Daout, S. Cesca, H. Vasyura-Bathke, and T. Dahm (2018), Grond - A probabilistic earthquake source inversion framework V. 1.0, GFZ Data Service, doi: 10.5880/GFZ.2.1.2018.003.

Hensch, M. (2009), On the interrelation of fluid-induced seismicity and crustal deformation at the Columbo Submarine Volcano (Aegean Sea, Greece), Doctoral thesis, 236 pp, Universität Hamburg, https://ediss.sub.uni-hamburg.de/volltexte/2010/4461/.

Hensch, M., C. Riedel, J. Reinhardt, and T. Dahm (2008), Hypocenter migration of fluid-induced earthquake swarms in the Tjörnes Fracture Zone (North Iceland), Tectonophysics, 447(1-4), 80-94, doi: 10.1016/j.tecto.2006.07.015.

Hooft, E. E. E., B. A. Heath, D. R. Toomey, M. Paulatto, C. B. Papazachos, P. Nomikou, J. V. Morgan, and M. R. Warner (2019), Seismic imaging of Santorini: Subsurface constraints on caldera collapse and present-day magma recharge, Earth and Planetary Science Letters, 514, 48-61, doi: 10.1016/j.epsl.2019.02.033.

Hooft, E. E. E., et al. (2017), Backarc tectonism, volcanism, and mass wasting shape seafloor morphology in the Santorini-Christiana-Amorgos region of the Hellenic Volcanic Arc, Tectonophysics, 712-713, 396-414, doi: 10.1016/j.tecto.2017.06.005.

Hübscher, C., M. Ruhnau, and P. Nomikou (2015), Volcano-tectonic evolution of the polygenetic Kolumbo submarine volcano/Santorini (Aegean Sea), Journal of Volcanology and Geothermal Research, 291, 101-111, doi: 10.1016/j.jvolgeores.2014.12.020.

Hübscher, C., M. Hensch, T. Dahm, A. Dehghani, I. Dimitriadis, M. Hort, and T. Taymaz (2006), Toward a risk assessment of central Aegean volcanoes, Eos, 87(39), doi: 10.1029/2006EO390002.

Kavanagh, J. L., A. J. Burns, S. Hilmi Hazim, E. P. Wood, S. A. Martin, S. Hignett, and D. J. C. Dennis (2018), Challenging dyke ascent models using novel laboratory experiments: Implications for reinterpreting evidence of magma ascent and volcanism, Journal of Volcanology and Geothermal Research, 354, 87-101, doi: 10.1016/j.jvolgeores.2018.01.002.

Kilias, S. P., et al. (2013), New insights into hydrothermal vent processes in the unique shallow-submarine arc-volcano, Kolumbo (Santorini), Greece, Scientific Reports, 3, 1-13, doi: 10.1038/srep02421.

Klaver, M., S. Carey, P. Nomikou, I. Smet, A. Godelitsas, and P. Vroon (2016), A distinct source and differentiation history for Kolumbo submarine volcano, Santorini volcanic field, Aegean arc, Geochemistry, Geophysics, Geosystems, 17(8), 3254-3273, doi: 10.1002/2016GC006398.

Konstantinou, K. I. (2020), Magma chamber evolution during the 1650 AD Kolumbo eruption provides clues about past and future volcanic activity, Scientific Reports, 10(1), 15423, doi: 10.1038/s41598-020-71991-y.

Konstantinou, K. I., and T.-Y. Yeh (2012), Stress field around the Coloumbo magma chamber, southern Aegean: Its significance for assessing volcanic and seismic hazard in Santorini, Journal of Geodynamics, 54, 13-20, doi: 10.1016/j.jog.2011.09.003.

Kühn, D., S. Heimann, M. P. Isken, E. Ruigrok, and B. Dost (2020), Probabilistic Moment Tensor Inversion for Hydrocarbon-Induced Seismicity in the Groningen Gas Field, The Netherlands, Part 1: Testing, Bulletin of the Seismological Society of America, 110(5), 2095-2111, doi: 10.1785/0120200099.

Kutterolf, S., et al. (2021), The medial offshore record of explosive volcanism along the central to eastern Aegean Volcanic Arc, part 1: Tephrostratigraphic correlations, Geochemistry, Geophysics, Geosystems, n/a(n/a), e2021GC010010, doi: 10.1029/2021GC010010.

Lahr, J. C., B. A. Chouet, C. D. Stephens, J. A. Power, and R. A. Page (1994), Earthquake classification, location, and error analysis in a volcanic environment: implications for the magmatic system of the 1989–1990 eruptions at redoubt volcano, Alaska, Journal of Volcanology and Geothermal Research, 62(1), 137-151, doi: 10.1016/0377-0273(94)90031-0.

Lomax, A., and A. Curtis (2001), Fast, probabilistic earthquake location in 3D models using Oct-Tree Importance sampling, in *Geophys. Res. Abstr.*, edited.

Lomax, A., J. Virieux, P. Volant, and C. Berge-thierry (2000), Probabilistic Earthquake Location in 3D and Layered Models, edited, pp. 101-134.

Maillot, B., S. Nielsen, and I. Main (1999), Numerical simulation of seismicity due to fluid injection in a brittle poroelastic medium, Geophysical Journal International, 139(2), 263-272, doi: 10.1046/j.1365-246x.1999.00933.x.

McVey, B. G., E. E. E. Hooft, B. A. Heath, D. R. Toomey, M. Paulatto, J. V. Morgan, P. Nomikou, and C. Papazachos (2019), Magma accumulation beneath Santorini volcano from P-wave tomography, c(Xx), 1-43, doi: 10.1130/G47127.1/4902160/g47127.pdf.

Moore, J. G. (2009), Structure and eruptive mechanisms at Surtsey Volcano, Iceland, Geological Magazine, 122(6), 649-661, doi: 10.1017/S0016756800032052.

Nomikou, P., C. Hübscher, and S. Carey (2019), The Christiana–Santorini–Kolumbo Volcanic Field, Elements, 15(3), 171-176, doi: 10.2138/gselements.15.3.171.

Nomikou, P., C. Hübscher, M. Ruhnau, and K. Bejelou (2016), Tectono-stratigraphic evolution through successive extensional events of the Anydros Basin, hosting Kolumbo volcanic field at the Aegean Sea, Greece, Tectonophysics, 671, 202-217, doi: 10.1016/j.tecto.2016.01.021.

Nomikou, P., S. Carey, D. Papanikolaou, K. Croff Bell, D. Sakellariou, M. Alexandri, and K. Bejelou (2012), Submarine volcanoes of the Kolumbo volcanic zone NE of Santorini Caldera, Greece, Global and Planetary Change, 90-91, 135-151, doi: 10.1016/j.gloplacha.2012.01.001.

Nomikou, P., S. Carey, K. L. C. Bell, D. Papanikolaou, K. Bejelou, K. Cantner, D. Sakellariou, and I. Perros (2014), Tsunami hazard risk of a future volcanic eruption of Kolumbo submarine volcano, NE of Santorini Caldera, Greece, Natural Hazards, 72(3), 1375-1390, doi: 10.1007/s11069-012-0405-0.

Ottemöller, L., and J. Havskov (2003), Moment magnitude determination for local and regional earthquakes based on source spectra, Bulletin of the Seismological Society of America, 93(1), 203-214, doi: 10.1785/0120010220.

Paige, C. C., and M. A. Saunders (1982), LSQR: Sparse linear equations and least squares problems, ACM Transactions of Mathematical Software, 8, 195-209.

Panza, G. F., and A. Saraò (2000), Monitoring volcanic and geothermal areas by full seismic moment tensor inversion: are non-double-couple components always artefacts of modelling?, Geophysical Journal International, 143(2), 353-364, doi: 10.1046/j.1365-246X.2000.01250.x.

Papanikolaou, D. (2013), Tectonostratigraphic models of the Alpine terranes and subduction history of the Hellenides, Tectonophysics, 595-596, 1-24, doi: 10.1016/j.tecto.2012.08.008.

Passarelli, L., E. Rivalta, S. Jónsson, M. Hensch, S. Metzger, S. S. Jakobsdóttir, F. Maccaferri, F. Corbi, and T. Dahm (2018), Scaling and spatial complementarity of tectonic earthquake swarms, Earth and Planetary Science Letters, 482, 62-70, doi: 10.1016/j.epsl.2017.10.052.

Petersen, G. M., S. Cesca, S. Heimann, P. Niemz, T. Dahm, D. Kühn, J. Kummerow, T. Plenefisch, A. the, and D. w. g. AlpArray-Swath (2021), Regional centroid moment tensor inversion of small to moderate earthquakes in the Alps using the dense

AlpArray seismic network: challenges and seismotectonic insights, Solid Earth, 12(6), 1233-1257, doi: 10.5194/se-12-1233-2021.

Phillipson, G., R. Sobradelo, and J. Gottsmann (2013), Global volcanic unrest in the 21st century: An analysis of the first decade, Journal of Volcanology and Geothermal Research, 264, 183-196, doi: 10.1016/j.jvolgeores.2013.08.004.

Preine, J., J. Karstens, C. Hübscher, P. Nomikou, F. Schmid, G. Crutchley, D. Papanikolaou, and T. H. Druitt (2021), Spatio-temporal evolution of the Christiana-Santorini-Kolumbo volcanic field, Aegean Sea, Geology, doi: 10.1130/G49167.1.

Rivalta, E., and T. Dahm (2006), Acceleration of buoyancy-driven fractures and magmatic dikes beneath the free surface, Geophysical Journal International, 166(3), 1424-1439, doi: 10.1111/j.1365-246X.2006.02962.x.

Rizzo, A. L., A. Caracausi, V. Chavagnac, P. Nomikou, P. N. Polymenakou, M. Mandalakis, G. Kotoulas, A. Magoulas, A. Castillo, and D. Lampridou (2016), Kolumbo submarine volcano (Greece): An active window into the Aegean subduction system, Scientific Reports, 6(May), 1-9, doi: 10.1038/srep28013.

Rizzo, A. L., et al. (2019), Geochemistry of CO2-Rich Gases Venting From Submarine Volcanism: The Case of Kolumbo (Hellenic Volcanic Arc, Greece), Frontiers in Earth Science, 7, 60.

Sakellariou, D., H. Sigurdsson, M. Alexandri, S. Carey, G. Rousakis, P. Nomikou, and D. Ballas (2017), Active tectonics in the Hellenic volcanic arc: The Kolumbo submarine volcanic zone, Bulletin of the Geological Society of Greece, 43(2), 1056-1063, doi: 10.12681/bgsg.11270.

Shapiro, S. A., E. Huenges, and G. Borm (1997), Estimating the crust permeability from fluid-injection-induced seismic emission at the KTB site, Geophysical Journal International, 131(2), F15-F18, doi: 10.1111/j.1365-246X.1997.tb01215.x.

Shapiro, S. A., R. Patzig, E. Rothert, and J. Rindschwentner (2003), Triggering of Seismicity by Pore-pressure Perturbations: Permeability-related Signatures of the Phenomenon, Pure and Applied Geophysics, 160(5), 1051-1066, doi: 10.1007/PL00012560.

Shcherbakov, R., D. L. Turcotte, and J. B. Rundle (2004), A generalized Omori's law for earthquake aftershock decay, Geophysical Research Letters, 31(11), doi: 10.1029/2004GL019808.

Shelly, D. R., S. C. Moran, and W. A. Thelen (2013), Evidence for fluid-triggered slip in the 2009 Mount Rainier, Washington earthquake swarm, Geophysical Research Letters, 40(8), 1506-1512, doi: 10.1002/grl.50354.

Sigmundsson, F., et al. (2015), Segmented lateral dyke growth in a rifting event at Bárðarbunga volcanic system, Iceland, Nature, 517(7533), 191-195, doi: 10.1038/nature14111.

Sigurdsson, H., S. Carey, M. Alexandri, K. Croff, C. Roman, D. Sakellariou, and P. Nomikou (2006), Marine Investigations of Greece ' s Santorini Volcanic Field, Eos, Trans. Am. Geophys. Un., 87(34).

Starostin, A. B., A. A. Barmin, and O. E. Melnik (2005), A transient model for explosive and phreatomagmatic eruptions, Journal of Volcanology and Geothermal Research, 143(1), 133-151, doi: 10.1016/j.jvolgeores.2004.09.014.

Tarasewicz, J., B. Brandsdóttir, R. S. White, M. Hensch, and B. Thorbjarnardóttir (2012), Using microearthquakes to track repeated magma intrusions beneath the Eyjafjallajökull stratovolcano, Iceland, Journal of Geophysical Research: Solid Earth, 117(B9), doi: 10.1029/2011JB008751.

Tilmann, F. J., I. Grevemeyer, E. R. Flueh, T. Dahm, and J. Goßler (2008), Seismicity in the outer rise offshore southern Chile: Indication of fluid effects in crust and mantle, Earth and Planetary Science Letters, 269(1-2), 41-55, doi: 10.1016/j.epsl.2008.01.044.

Vidale, J. E., and P. M. Shearer (2006), A survey of 71 earthquake bursts across southern California: Exploring the role of pore fluid pressure fluctuations and aseismic slip as drivers, Journal of Geophysical Research: Solid Earth, 111(B5), doi: 10.1029/2005JB004034.

Waldhauser, F. (2001), HypoDD - A Program to Compute Double-Difference Hypocenter Locations, US Geol. Surv. Open File Rep. 01-113, 1-25, doi: http://geopubs.wr.usgs.gov/open-file/of01-113/.

Waldhauser, F., and W. L. Ellsworth (2000), A double-difference Earthquake location algorithm: Method application to the northern Hayward fault, Bull. Seismol. Soc. Am., 90, 1353-1368, doi: 10.1785/0120000006.

Wang, R. (1999), A simple orthonormalization method for stable and efficient computation of Green's functions, Bulletin of the Seismological Society of America, 89(3), 733-741, doi: 10.1785/BSSA0890030733.

Yukutake, Y., H. Ito, R. Honda, M. Harada, T. Tanada, and A. Yoshida (2011), Fluid-induced swarm earthquake sequence revealed by precisely determined hypocenters and focal mechanisms in the 2009 activity at Hakone volcano, Japan, Journal of Geophysical Research: Solid Earth, 116(B4), doi: 10.1029/2010JB008036.